The degradation and performance of electrospun supramolecular vascular scaffolds examined upon in vitro enzymatic exposure

Acta Biomaterialia 92 (2019) 48–59

Contents lists available at ScienceDirect

Acta Biomaterialia

journal homepage: www.elsevier.com/locate/actabiomat

Full length article

The degradation and performance of electrospun supramolecular vascular scaffolds examined upon *in vitro* enzymatic exposure

E.E. van Haaften [a,b,1], R. Duijvelshoff [a,b,1], B.D. Ippel [a,b], S.H.M. Söntjens [c], M.H.C.J. van Houtem [c], H.M. Janssen [c], A.I.P.M. Smits [a,b], N.A. Kurniawan [a,b], P.Y.W. Dankers [a,b], C.V.C. Bouten [a,b,*]

[a] Eindhoven University of Technology, Department of Biomedical Engineering, PO Box 513, 5600 MB Eindhoven, The Netherlands
[b] Institute for Complex Molecular Systems (ICMS), PO Box 513, 5600 MB Eindhoven, The Netherlands
[c] SyMO-Chem B.V., Den Dolech 2, 5612 AZ Eindhoven, The Netherlands

ARTICLE INFO

Article history:
Received 16 January 2019
Received in revised form 11 May 2019
Accepted 15 May 2019
Available online 17 May 2019

Keywords:
Tissue engineering
Vascular graft
Electrospinning
Lipase
Bulk and surface erosion

ABSTRACT

To maintain functionality during *in situ* vascular regeneration, the rate of implant degradation should be closely balanced by neo-tissue formation. It is unknown, however, how the implant's functionality is affected by the degradation of the polymers it is composed of. We therefore examined the macro- and microscopic features as well as the mechanical performance of vascular scaffolds upon *in vitro* enzymatic degradation. Three candidate biomaterials with supramolecularly interacting bis-urea (BU) hard blocks ('slow-degrading' polycarbonate-BU (PC-BU), 'intermediate-degrading' polycarbonate-ester-BU (PC(e)-BU), and 'fast-degrading' polycaprolactone-ester-BU (PCL-BU)) were synthesized and electrospun into microporous scaffolds. These materials possess a sequence-controlled macromolecular structure, so their susceptibility to degradation is tunable by controlling the nature of the polymer backbone. The scaffolds were incubated in lipase and monitored for changes in physical, chemical, and mechanical properties. Remarkably, comparing PC-BU to PC(e)-BU, we observed that small changes in macromolecular structure led to significant differences in degradation kinetics. All three scaffold types degraded via surface erosion, which was accompanied by fiber swelling for PC-BU scaffolds, and some bulk degradation and a collapsing network for PCL-BU scaffolds. For the PC-BU and PC(e)-BU scaffolds this resulted in retention of mechanical properties, whereas for the PCL-BU scaffolds this resulted in stiffening. Our *in vitro* study demonstrates that vascular scaffolds, electrospun from sequence-controlled supramolecular materials with varying ester contents, not only display different susceptibilities to degradation, but also degrade via different mechanisms.

Statement of Significance

One of the key elements to successfully engineer vascular tissues *in situ*, is to balance the rate of implant degradation and neo-tissue formation. Due to their tunable properties, supramolecular polymers can be customized into attractive biomaterials for vascular tissue engineering. Here, we have exploited this tunability and prepared a set of polymers with different susceptibility to degradation. The polymers, which were electrospun into microporous scaffolds, displayed not only different susceptibilities to degradation, but also obeyed different degradation mechanisms. This study illustrates how the class of supramolecular polymers continues to represent a promising group of materials for tissue engineering approaches.

1. Introduction

There is a large clinical demand for small-diameter vascular conduits to treat patients suffering from cardiovascular disease or end-stage kidney disease [1,2]. Vascular conduits are required for coronary artery bypass grafting, for lower limb revascularization procedures, and for use in arteriovenous access shunts that are applied for hemodialysis. To date, the golden standard for arte-

* Corresponding author at: Eindhoven University of Technology, Department of Biomedical Engineering, PO Box 513, 5600 MB Eindhoven, The Netherlands.
E-mail address: C.V.C.Bouten@tue.nl (C.V.C. Bouten).
[1] These authors contributed equally to this study.

https://doi.org/10.1016/j.actbio.2019.05.037
1742-7061/

rial replacement remains the use of the patient's own vasculature (e.g., internal thoracic artery, radial artery or great saphenous vein), mainly because the tissue is biocompatible, has matching mechanical properties, and possesses a non-thrombogenic endothelium. Despite these advantages, autologous replacement is often not an option, because many patients lack appropriate vessels due to vascular disease or previous harvest. As a result, there is a growing demand for alternative vascular substitutes. However, currently available small-diameter vascular substitutes (<6 mm) have been characterized by poor biocompatibility, thrombosis, and intimal hyperplasia leading to stenosis [3–5]. To overcome these problems and address the need for small-diameter vascular conduits, tissue engineering (TE) approaches are being investigated to offer an alternative.

Various approaches for vascular TE using cell-laden or acellular biodegradable scaffolds (either of biological or synthetic origin) have been widely explored [6]. Recent developments have led to an increased focus on *in situ* TE using cell-free synthetic biodegradable scaffolds, also because this approach represents a clinically appealing strategy due to the off-the-shelf availability of implant materials [7]. *In situ* TE largely depends on the host's capacity to colonize and populate the scaffold with endogenous cells that produce extracellular matrix (ECM). It also requires scaffolds that have sufficient strength to take over artery functionality immediately upon implantation, thereby withstanding the high mechanical demands imposed by the arterial high-pressure circulation. Furthermore, maintenance of the mechanical integrity during the build-up of neo-tissue by the host, while the scaffold is being degraded, is essential to avoid graft failure [8]. Hence, the scaffold must degrade in pace with neo-tissue formation to allow for a safe and mechanically stable transition from scaffold implant to living autologous blood vessel.

During the process of degradation, both the macro- and microscopic properties of the scaffold are altered. However, these alterations, as well as their potential effects on the scaffold functionality, particularly in terms of mechanical performance, are not well understood. Biodegradable polymers are degraded through four primary pathways, namely hydrolytic, oxidative, enzymatic, and physical degradation [9]. Of these, hydrolysis, which can be catalyzed by enzymes such as lipase and esterase, represents the major degradation mechanism in polymeric scaffolds [10,11]. Upon contact with water, polymer covalent bonds break, leading to smaller chains that ultimately can be eliminated from the body. Both polyesters and polycarbonates are susceptible to hydrolysis, with polyesters generally being more susceptible than polycarbonates [9].

A specific class of synthetic biomaterials are supramolecular polymers. This class is attractive for vascular TE as these materials can be customized for specific vascular applications through the incorporation of bioactive moieties, non-cell-adhesive components, or specific cell-attracting peptides [12–15]. Moreover, their properties in general are highly tunable [16,17]. For the present study we have exploited this tunability and have prepared a set of polymers with supramolecularly interacting bis-urea (BU) units in their structure. The polycarbonate-BU (PC-BU), polycarbonate-ester-BU (PC(e)-BU), and polycaprolactone-BU (PCL-BU) materials are segmented thermoplastic elastomers (TPEs) with a sequence-controlled molecular structure: the macromolecules have an exact alternation of BU hard blocks and polycarbonate (PC), polycarbonate-ester (PC(e)), or polycaprolactone ester (PCL) soft blocks. Accordingly, the molecular nature of the hard and soft blocks is the same along the length of the polymer chain for each of the three materials. On the one hand, these biomaterials are therefore expected to be similarly soft, tough, and non-cytotoxic. On the other hand, however, the pinpointed differences in the nature of the soft block (i.e., the ester/carbonate content as well as the difference between PCL and PC) are expected to translate to a variation in degradation behavior. Additionally, these differences may also modulate the thermal and mechanical properties of the resulting biomaterials.

Previously, PC-BU-based scaffolds have been shown to successfully function as implanted tissue-engineered heart valves in sheep. The porous scaffolds were still (partly) present after 1 year *in vivo* [18]. In contrast, PCL-BU-based scaffolds that were implanted as interposition grafts into the abdominal aorta of a rat model completely degraded in less than 2 months [19]. The application of PCL-BU in porous implants for cardiovascular *in situ* TE therefore seems precluded. However, when subcutaneously implanted as solid discs in rats, this material was only minimally affected by degradation after 1.5 months [20]. These differences in the degradation kinetics presumably originate from the different processing methods, shapes, and morphologies that have been used for the particular implants, or from the different biological responses that depend on the implantation site and species [21,22]. For *in situ* TE, the overall functionality of the implant is affected by degradation, so the observed variations in *in vivo* results underscore the importance of gaining more insight into the effect of degradation on the overall properties, including the mechanical properties, of the implant. It is then also important to study the degradation at the level of the actually implanted porous scaffold, and not merely at the level of the biomaterial itself.

Accordingly, we have examined the *in vitro* degradation of electrospun scaffolds of PC-BU and PCL-BU more closely, and have also included the newly introduced PC(e)-BU material in our assessment. Apart from studying differences in degradation kinetics, we have also investigated the functional performance of the porous scaffolds upon degradation. In our approach, we used lipase-enzyme accelerated *in vitro* degradation protocols to mimic the actual *in vivo* degradation of the implants. Particularly, vascular scaffolds, electrospun from the three candidate BU-materials with varying ester contents, were exposed to lipase solutions, thereby accelerating the degradation process. At various time points (up to 9 days) the scaffolds were characterized with regard to their physical, chemical and mechanical properties. More specifically, the mass loss and the thickness of the scaffolds have been monitored, as well as the mechanical properties of the scaffolds (by biaxial tensile testing). Furthermore, fiber morphology within the scaffold (with SEM), the thermal behavior (by DSC) and the molecular weight (by GPC) of the degrading scaffold materials have been examined (Fig. 1).

2. Materials and methods

2.1. Scaffold preparation

2.1.1. Polymer synthesis

PC-BU and PCL-BU were synthesized using 3-step synthetic procedures [18,23]. Briefly, the syntheses of PC-BU and PCL-BU start from polyhexylcarbonate diol and polycaprolactone diol, respectively, with both these telechelic prepolymer diols having a M_n of 2 kDa. In the first step, the diols were capped by reaction with either 6-((*tert*-butoxycarbonyl)amino)hexyl 1*H*-imidazole-1-carboxylate applying DBU-base reagent (for PC-BU) or 6-((*tert*-butoxycarbonyl)amino)hexanoic acid employing DCC coupling reagent (for PCL-BU). Next, the resulting N-Boc protected telechelic prepolymers were deprotected with trifluoracetic acid (TFA), and finally, in the third step, the amine functional prepolymers were converted and chain-extended with 1,4-butanediisocyanate. The synthesis of the PC(e)-BU material has also been performed in a

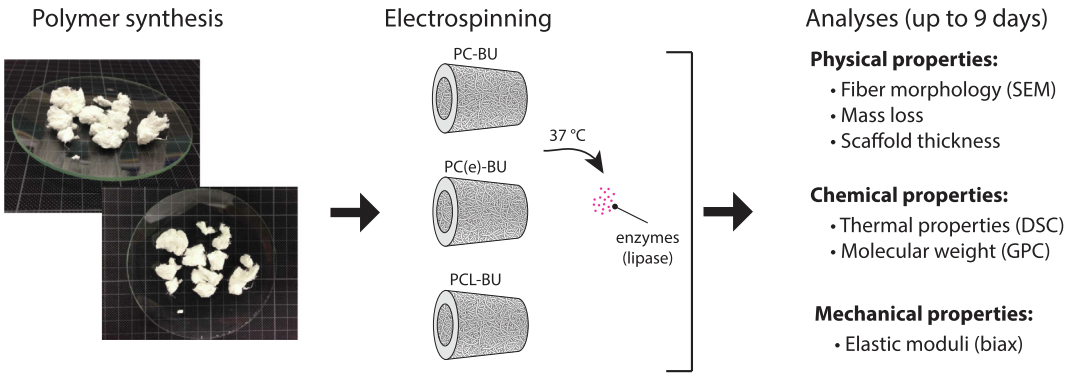

Fig. 1. Schematic overview of the experimental design and readouts. Three candidate biomaterials ('slow-degrading' polycarbonate BU (PC-BU), 'intermediate-degrading' polycarbonate-ester BU (PC(e)-BU), and 'fast-degrading' polycaprolactone ester BU (PCL-BU)) were synthesized and electrospun into microporous vascular scaffolds. The scaffolds were incubated in a lipase solution at 37 °C and were monitored for changes in physical, chemical, and mechanical properties.

3-step approach, and is outlined in detail in Supplementary Information SI.1.

2.1.2. Electrospinning

Tubular scaffolds (ø 3 mm, 5 μm fibers) and scaffold sheets (10×10 cm^2, 5 μm fibers) were electrospun from three different polymer solutions containing $CHCl_3$ (Sigma-Aldrich, 372978), and MeOH (VWR Chemicals, 20903.368) or HFIP (Fluorochem, 920-66-1) (Table 1). The polymer solutions were delivered via a positively charged needle onto a negatively charged rotating mandrel (ø 3 mm at 500 rpm for the tubes (6 cm deposition distance) and ø 35 mm at 100 rpm for the sheets (10 cm deposition distance)) in a climate-controlled cabinet (EC-CLI, IME Technologies, Geldrop, the Netherlands) at 23 °C and 30% relative humidity. To ensure comparable fiber diameter and fiber organization between the three candidate materials, they were produced according to the settings in Table 1. After removal from the mandrel, the resulting scaffolds tubes and sheets were placed under vacuum for 16 h at 23 °C according to routinely-used protocols to remove any residual solvent [15,24]. For the experiments, 10 mm pieces were cut from the tubular meshes, and 10×10 mm^2 pieces were cut from the scaffold sheets. Prior to the degradation experiments, the samples were placed in sterile H_2O and centrifuged for 10 min at 4500 rpm to wet the materials.

2.2. Lipase accelerated degradation experiments

The prepared scaffolds were incubated in a 3 ml lipase solution in water (from *Thermomyces lanuginosus*, Sigma Aldrich, L0777) at concentrations ranging from 10 U/ml to 1000 U/ml at 37 °C. At each time point, scaffolds were washed 3 times with sterile H_2O, snap-frozen in liquid nitrogen, and stored at −80 °C until analysis, unless stated otherwise. Based on this protocol, three different types of degradation experiments were performed.

Table 1
Electrospinning settings to produce vascular scaffolds from the three candidate polymers.

Settings	Material group		
	PC-BU	PC(e-)-BU	PCL-BU
wt% polymer	7.5	13.3	15.0
Solvent (w/w)	99.5:0.5 ($CHCl_3$:MeOH)	95:5 ($CHCl_3$:HFIP)	98:2 ($CHCl_3$:MeOH)
Flow rate (μl/min)	40	45	35
Needle-to-mandrel (cm)	25	16	16
Needle voltage (kV)	16	17	17
Mandrel voltage (kV)	−1	−1	−1

2.2.1. Validation experiments

In the first set of experiments, pre-wetted scaffold meshes (10×10 mm^2, $n = 3$ for every condition and time point) of each material were incubated at two different enzyme concentration conditions (50 U/ml and 100 U/ml lipase solution). To make direct correlations between the sample's physical properties (i.e., scaffold thickness, mass loss, and fiber morphology, see Section 2.3.1), each analysis was performed on each individual sample at predetermined end points (0, 8, 28, 72 h).

2.2.2. Scaffold degradation and functional performance

For the second experiment, different degradation protocols were used for each material, i.e., different enzyme concentrations and/or durations were employed for each material. The 10 mm tubular PC-BU scaffolds were incubated with a 500 U/ml lipase solution up to 9 days (with intermediate time points at 3 and 6 days), whereas the PC(e)-BU and PCL-BU scaffolds were incubated with 30 U/ml and 10 U/ml lipase solution, respectively, up to 6 days (with intermediate time points at 2 and 4 days). The lipase solution was refreshed every 2–3 days to maintain enzyme activity [25,26]. During enzyme exposure, the scaffolds were monitored for their physical properties (i.e., fiber morphology, mass loss, and thickness, Section 2.3.1), chemical properties (i.e., thermal and molecular analysis, Section 2.3.2), and mechanical properties (Section 2.3.3). For each analysis, a total of three scaffolds per material per time point were included (see the detailed experimental scheme in Supplementary Information SI.2).

2.2.3. Functional performance at high scaffold degradation

In the last set of experiments, the tubular PC-BU scaffolds were incubated with a 1000 U/ml lipase solution for 20 days, while the PC(e)-BU and PCL-BU scaffolds were incubated with a 100 U/ml lipase solution for 6 and 9 days, respectively. After enzyme exposure, the sample's mass loss (Section 2.3.1) and mechanical properties (Section 2.3.3) were characterized ($n = 3$ per analysis).

2.3. Experimental readouts

2.3.1. Physical properties

Fiber morphology. The scaffold fiber morphology was examined by scanning electron microscopy (SEM) (Quanta 600F, FEI, Hillsboro, OR, USA). Scaffolds were dried under vacuum, gold-sputtered, and visualized in low vacuum atmosphere with an electron beam of 5 kV. Average fiber diameters were measured from SEM images

using ImageJ (v1.48, U.S. NIH, Bethesda, MD, USA). At least 20 individual fibers of each scaffold were measured. Fiber directionality and distribution of directionality was quantified using previously developed software [27]. The % of aligned fibers was calculated by fitting a Gaussian distribution with an additional baseline onto the histogram of the detected fiber directions. The fraction of aligned fibers was defined as the fraction of fibers belonging to the Gaussian distribution.

Mass loss. Scaffolds were lyophilized for 3 h, and then immediately weighed using a digital balance (XS105 dual-range analytical balance, Mettler Toledo, Switzerland). The remaining mass after scaffold degradation was normalized against the initial scaffold mass.

Scaffold thickness. Scaffold thickness was measured at two opposing edges (>3 locations/side) using a digital microscope (Keyence VHX-500FE, Itasca, IL, USA). For the validation experiment (Section 2.2.1 10×10 mm^2 sheets), the scaffold thickness was measured after lyophilisation, and the scaffolds dry thickness after degradation was normalized by the initial scaffold thickness. For the other experiments (Sections 2.2.2 and 2.2.3, ø3 mm $\times$ 10 mm tubes), the scaffold thickness was measured directly after washing, i.e., in wet conditions, and no normalization step was performed.

2.3.2. Chemical properties

Differential scanning calorimetry analysis (DSC). Directly after washing, samples were dried under vacuum and stored at room temperature. DSC measurements were performed on a DSC Q2000 (TA instruments, USA). Electrospun samples were weighed, and subsequently hermetically sealed in Tzero aluminum pans. The samples were first cooled to −80 °C and then subjected to two heating/cooling cycles from −80 °C to 160 °C with a rate of 10 °C/min. The presented melting peak (defined as the peak maximum) and melting enthalpy (defined as the peak area) were determined from the first heating run using Universal Analysis software (V4.5A, TA Instruments).

Gel permeation chromatography (GPC). Scaffold samples for GPC were dissolved at a concentration of 1 mg/ml in dimethylformamide, supplemented with 10 mM LiBr and 0.3% (v/v) H_2O. Prior to the measurements, the sample solutions were filtered using a 0.2 μm regenerated cellulose filter. Weight-averaged molecular weights (M_w) and number-averaged molecular weights (M_n) relative to poly(ethylene glycol) standards were determined with a Varian/Polymer Laboratories PL-GPC 50 Plus instrument (Varian Inc., Palo Alto, CA, USA) operated at 50 °C, equipped with a Shodex GPC KD-804 column (Shodex, Tokyo, Japan).

2.3.3. Mechanical properties

The mechanical properties of the scaffolds were characterized immediately after washing in wet conditions at 37 °C in a biaxial tensile setup (CellScale Biomaterial Testing, Waterloo, Canada; equipped with a 1500 or 5000 mN load cell). The scaffolds were longitudinally opened and 7×7 mm^2 samples were cut. After the scaffold thickness measurement (Section 2.3.1.3), the sample's circumferential and axial directions were aligned with the actuators and mounted. Prior to the test, the samples were sprayed with graphite to facilitate optical strain analysis. After 10 cycles of uniaxial strain up to 10% in each direction, the samples were equibiaxially stretched at a strain rate of 100% min^{-1} until 100%. Assuming incompressibility and plane-stress conditions, Cauchy stress–stretch curves were calculated from the force and displacement measurements. As a measure of stiffness, the slope at physiological stretch values of 1.05 and 1.15 stretch was calculated [28].

2.4. Statistical analysis

All data are expressed as mean ± standard deviation. To assess the overall effect of incubation time and the relationship between mass loss and scaffold thickness, the data were analyzed using linear regression in Matlab R2016b (The Mathworks, Natick, MA). To evaluate differences between the different time points, a Kruskal-Wallis test, followed by Dunn's multiple comparison test, was performed in Prism (Graphpad Software v5.04, La Jolla, CA, USA). Statistical differences were considered to be significant for p-values <0.05.

3. Results

3.1. Materials and scaffolds before degradation

The synthesis of the polymers resulted in biomaterials with the macromolecular structures as depicted in Fig. 2A. The sequence-controlled TPEs have identical bis-urea (BU) hard blocks, similar soft block lengths (M_n of about 2.5–2.8 kg/mol), but varying poly (ester/carbonate) soft block compositions. Supplementary Information SI.3 contains information on the bulk thermal and mechanical properties of the three investigated biomaterials. Electrospinning of the biomaterials resulted in fibrous scaffolds with similar fiber diameters of about 5 μm (Fig. 2B, C, Table 2). All scaffold groups exhibited at the outer side some degree of fiber alignment in the axial direction, which became more pronounced in the thicker scaffolds (Table 2, Fig. SI2A). The luminal side of the pristine scaffolds was characterized by a porous and isotropic fiber network (Fig. 2C, upper panel). Slight differences in the smoothness of fibers between the three materials were observed, which are most likely due to the electrospinning process (Fig. 2C, lower panel).

3.2. Validation experiments

We first studied the degradation kinetics of the three materials, and found that the degradation profiles due to exposure of the scaffolds to 100 U/ml lipase solutions clearly differed (Fig. 3A). Similar results were obtained using 50 U/ml lipase (Supplementary Information SI.4). After 72 h incubation, the PC-BU scaffolds had hardly lost any mass (~5%), while the PC(e)-BU and the PCL-BU scaffolds had lost about 50% of their original mass (Fig. 3A). PC (e)-BU showed kinetics intermediate to those of PC-BU and PCL-BU. Only at the earliest time points it gave similar results as found for PC-BU, the material that it closely resembles molecularly. These data demonstrate that the susceptibility of the BU-based supramolecular polymeric scaffolds to enzymatic degradation can be robustly tuned.

Next, we examined and compared the fiber morphology, sample thickness, and mass loss of the scaffolds, as subjected to the two enzyme concentrations (Fig. 3B–E). For all three materials, it was observed that the varying enzyme concentrations did not affect the relationship between sample thickness and mass loss, indicating that a similar degradation state of a scaffold (i.e., a state of a scaffold of a certain mass loss coupled to a certain scaffold thickness and a certain fiber thickness, all for a particular biomaterial) can be attained using different lipase concentrations (Fig. 3C–E). This result also shows that the degradation rate does not seem to affect the degradation states that a scaffold traverses during its degradative process. Finally, a pair of scaffold samples was taken from each material group that had attained comparable degradation states after different incubation times with different enzyme concentrations (indicated by the arrowheads in Fig. 3C–E). SEM analysis of these sample pairs show very similar fiber morpholo-

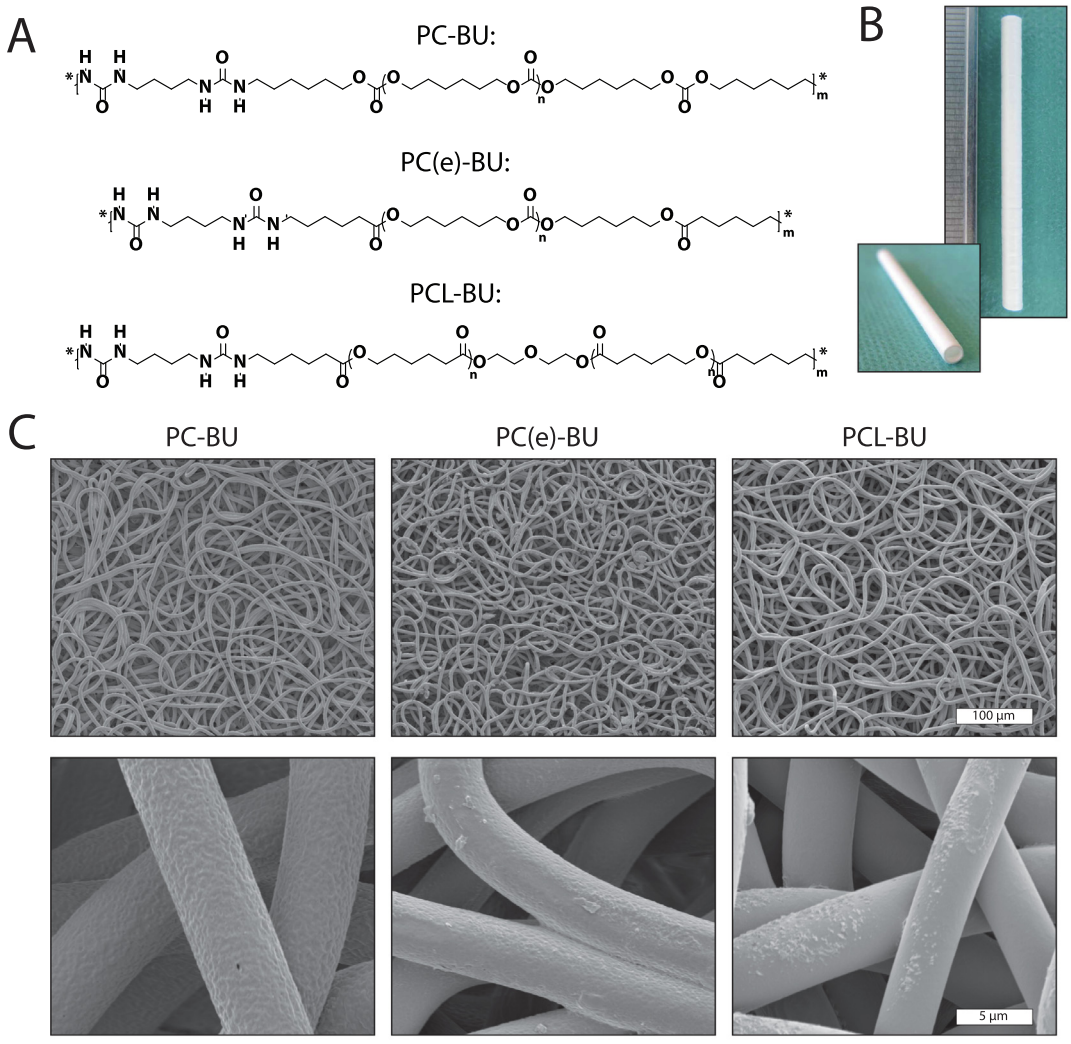

Fig. 2. Materials and scaffolds before degradation. (A) Macromolecular structures of the employed supramolecular polymers: polyhexylcarbonate bis-urea (PC-BU), polyhexylcarbonate-ester bis-urea (PC(e)-BU), and polycaprolactone bis-urea (PCL-BU). (B) Gross appearance of a vascular scaffold electrospun from PC-BU with 3 mm inner diameter (ruler ticks 1 mm). (C) Representative scanning electron microscopy images of electrospun BU-scaffolds (*upper panel*, scale bar = 100 µm; *lower panel*, scale bar = 5 µm).

Table 2
Properties of the electrospun vascular BU-scaffolds.

Properties		Material group		
		PC-BU	PC(e-)-BU	PCL-BU
% ester/carbonate in soft block		0/100	ca. 11/89	100/0
Fiber diameter (µm)	Inside	5.3 ± 0.1	4.4 ± 0.1	4.7 ± 0.0
	Outside	5.9 ± 0.2	4.5 ± 0.2	4.4 ± 0.0
% Aligned fibers (axial direction)	Inside	12 ± 9	20 ± 14	10 ± 8
	Outside	42 ± 21	63 ± 19	57 ± 7
Wall thickness (µm)		339 ± 29	726 ± 65	668 ± 58
Lumen diameter (mm)		3	3	3

gies for each material (Fig. 3B), confirming that equivalent degradation states can be obtained by exposure to different enzyme concentrations and incubation times. These results validate our approach of examining and comparing biomaterial scaffolds as acquired by *in vitro* accelerated degradation protocols that apply different enzyme concentrations.

3.3. Monitoring scaffold mass and morphology upon degradation

The PC-BU, PC(e)-BU, and PCL-BU scaffolds were incubated with a 500 U/ml, 30 U/ml, and 10 U/ml lipase solution, respectively, allowing examination of the degradation states of these biomaterial scaffolds within a similar experimental time frame. The remaining mass of all scaffolds decreased during lipase exposure (Fig. 4A, see also Table SI3 in the Supplementary Information for data on statistical significance). This coincided with a decrease in the scaffold thickness for both the PC(e)-BU as well as the PCL-BU scaffolds (Fig. 4B). In contrast, the thickness of PC-BU scaffolds remained constant despite the mass loss. The scaffold density, defined as the calculated ratio between scaffold mass and thickness, decreased with longer degradation times for the PC-BU and PC(e)-BU scaffolds. In contrast, the density of the PCL-BU scaffolds largely remained constant over time, or even increased to a minor extent (Fig. 4C).

The samples were next examined at the microscopic fiber scale. Upon degradation, clear changes in the fiber morphology were observed for the three biomaterials, most strikingly for the PCL-BU scaffolds that often (but not always) showed an erosion-like

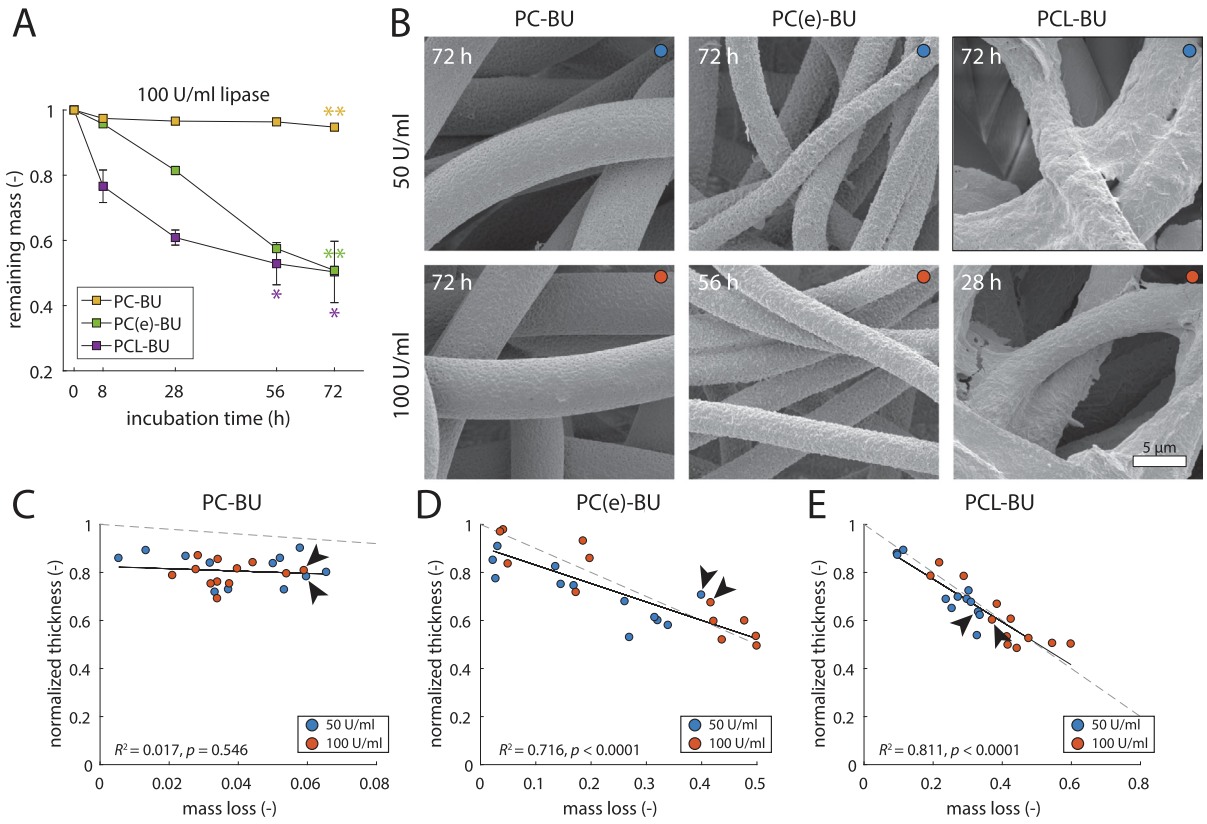

Fig. 3. Validation experiments. (A) Remaining mass fraction of electrospun BU-scaffolds during degradation by 100 U/ml lipase incubation (*error bars* for PC-BU and PC(e)-BU are in the order of graph point size, *asterisks* indicate statistical difference compared to pristine scaffolds at 0 h ($^{*}p < 0.05$, $^{**}p < 0.01$)). (B) Scanning electron microscopy (SEM) images of the BU-scaffolds after 50 U/ml (*upper panel*) and 100 U/ml (*lower panel*) lipase incubation for 28–72 h (scale bar = 5 µm). (C–E) Relationships between sample thickness and mass fraction (in dry state) of the BU-scaffolds in 50 U/ml (*blue dots*) and 100 U/ml (*red dots*) lipase incubation up to 72 h (the *solid line* represents the linear regression through the data points with associated R^2 and *p*-value). The scaffold thickness is normalized to its initial thickness. The theoretical relationship between thickness and mass fraction (assuming constant density) is represented by the *dotted line*. *Arrowheads* indicate the samples further examined with SEM in (B). (For interpretation of the references to colour in this figure legend, the reader is referred to the web version of this article.)

appearance with small pits in the fibers (Fig. 5A). Quantification of the fiber diameters from SEM images revealed a constant, even slight increase of fiber diameter in the PC-BU scaffolds, although this was not statistically significant (Fig. 5B). In contrast, the fiber diameters in PC(e)-BU and PCL-BU scaffolds gradually and significantly decreased with longer enzymatic degradation.

To assess the homogeneity of fiber degradation in the samples, the fiber diameter as a function of mass loss was plotted (Fig. 5C). If the material degrades homogeneously via surface erosion, the relation between the decrease in fiber diameter and mass loss is expected to follow a quadratic profile (dotted lines in Fig. 5C, see Supplementary Information SI.6). The PCL-BU and PC(e)-BU fibers degrade corresponding to this profile, although this is less clear for the PC(e)-BU material. On the other hand, the profile for the PC-BU fibers seems to show a slight positive correlation with mass loss, suggesting fiber swelling

3.4. Monitoring thermal properties and molecular weight upon degradation

In further analyses, we checked whether enzymatic degradation resulted in changes in the thermal properties and the molecular weight of the remaining scaffold materials. The trace of the first heating run from the DSC measurements on the electrospun scaffolds typically showed two distinct transitions (Fig. 6A). The first melting transition corresponds to the melting of the polymer soft phase (i.e., PC, PC(e) or PCL), whereas the second transition (peak at >100 °C) corresponds to the melting of the BU hard phase. Only for PCL-BU an additional third transition was observed at about 60 °C (see Supplementary Information SI.3 for related details). The melting enthalpy as well as the melting temperature of the BU-melt did not significantly change for the three polymers upon degradation, even though they tended to decrease with enzymatic degradation, especially for the PCL-BU polymer (Fig. 6B, C).

Finally, the GPC measurements indicated that the molecular weight of the remaining PC-BU and PC(e)-BU materials did not change with degradation. For PCL-BU, however, the molecular weight of the remaining material slightly and significantly decreased (Fig. 6D). Apparently, the bulk material in the fibers is not affected by lipase and/or water for PC-BU and PC(e)-BU, while it degrades for PCL-BU.

3.5. Monitoring scaffold mechanical properties upon degradation

To assess the mechanical performance of the scaffolds after degradation, biaxial tensile testing was performed. All scaffolds showed some degree of non-linear, anisotropic mechanical behavior (Fig. 7A). In particular, the PC-BU scaffolds were stiffer in the circumferential direction at higher levels of stretch, whereas the PC(e)-BU and PCL-BU scaffolds were stiffer in the axial direction. Irrespective of the polymer backbone, the pristine materials showed E-moduli in the same range of about 1 MPa, confirming

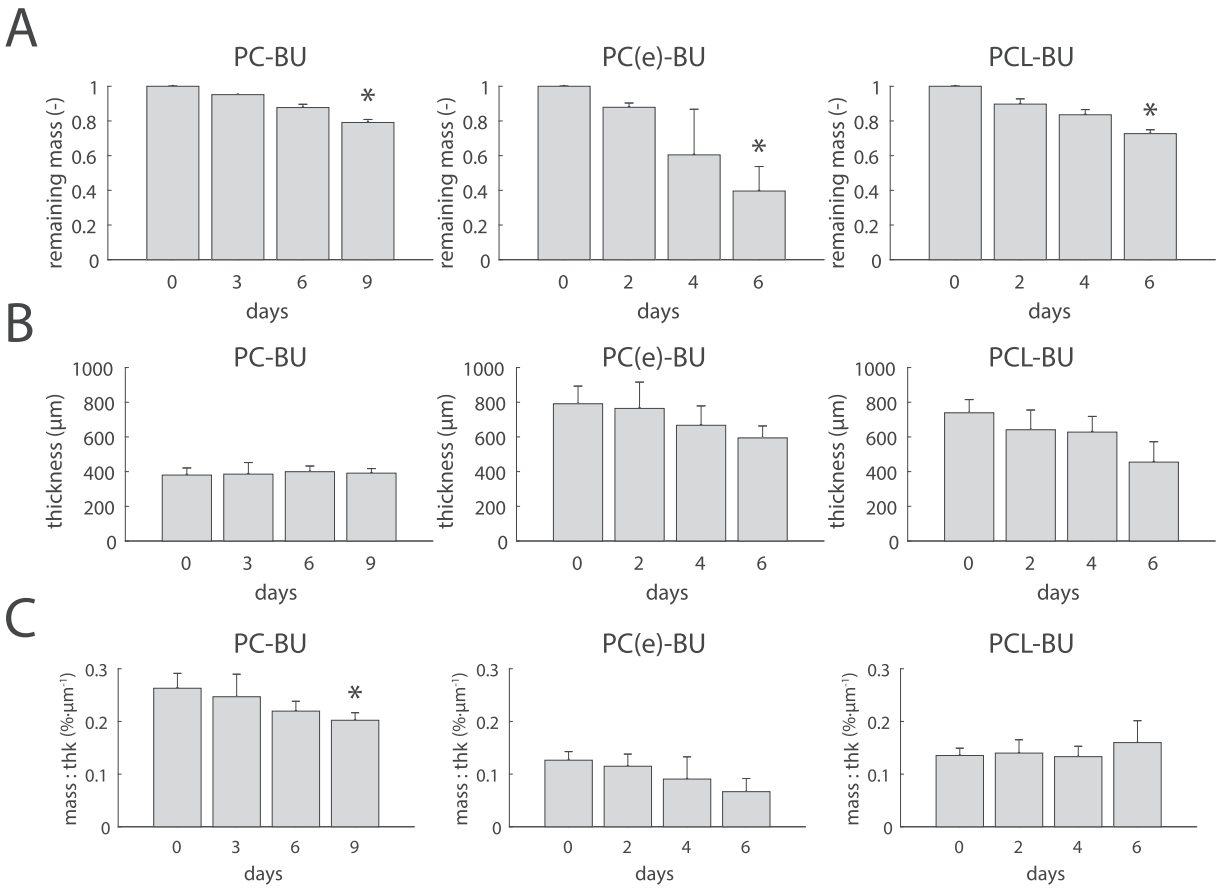

Fig. 4. Physical degradation on the scaffold-scale. (A) Remaining mass fraction (in dry state), (B) thickness (in wet state), and (C) density (i.e., ratio between remaining mass and thickness) of electrospun BU-scaffolds during lipase incubation (PC-BU in 500 U/ml, PC(e)-BU in 30 U/ml, and PCL-BU in 10 U/ml). *Asterisks* indicate statistical difference compared to day 0 ($^{*}p < 0.05$, see also Table SI3 in the Supplementary Information for the overall effect of incubation time).

the similarity between the mechanical properties of the three biomaterials. Interestingly, the PCL-BU scaffolds became stiffer upon degradation in the axial direction, even at a high degree of degradation (Fig. 7B, Table 3). This stiffening effect was also observed, though only at higher stretches, for PCL-BU scaffolds that were deliberately electrospun to acquire fibers in the circumferential direction (see Supplementary Information SI.7 for details). The PC(e)-BU scaffolds largely maintained their mechanical performance up to 40% of remaining mass (Fig. 7B). However, these scaffolds abruptly lost their tensile properties at higher levels of degradation (Table 3). The behavior of the PC-BU scaffolds was less clear, but it seemed that their E-moduli stayed in the same range upon degradation (Fig. 7B, Table 3).

4. Discussion

In *in situ* TE, the degradation rate of the porous implant should complement the rate at which new tissue is formed to warrant a sustained mechanical function. Patient characteristics (e.g., immune response and age), location of implantation [21,22], and the specific nature of the scaffold (e.g., shape, chemical composition, physical properties) determine the degradation rate of the implant. Ultimately, the *in situ* TE process is aimed at, and must lead to, a safe and successful transition from synthetic conduits into neo-vessels in which no scaffold is present anymore. Importantly, during this transition, the mechanical integrity of the implant must be maintained at all times to prevent premature graft failure. Here, we therefore have dissected how enzymatic hydrolytic degradation affects the physical properties and mechanical performance of scaffolds as electrospun from the candidate supramolecular BU-materials PC-BU, PC(e)-BU, and PCL-BU. We have demonstrated that the electrospun scaffolds degrade in different ways, and based on the findings we propose a material dependent degradation mechanism for the scaffolds that is schematically visualized in Fig. 8.

The examined BU-materials have a sequence-controlled molecular structure, and in this respect they deviate from polycarbonate, polyester, or co-polycarbonate/ester BU-materials that are prepared in two-step one-pot procedures [29,30]. The latter TPE materials have a macromolecular structure that is determined by statistics, and that accordingly has a range in hard and soft block identities, implying that all macromolecules composing a certain material have a different molecular microstructure. These materials also contain urethane groups, while PC-BU, PC(e)-BU, and PCL-BU do not. Each of the three sequence-controlled biomaterials is composed of macromolecules that are very much alike, and that only vary in macromolecular length. Accordingly, the degradation products of PC-BU, PC(e)-BU, and PCL-BU can be expected to be less diverse than those for the one-pot produced BU-polyurethanes. The high control over their molecular structure, leading to a high control over their specific properties, make sequence-controlled materials attractive for assessing their performance in biomedical applications, for example in *in situ* TE.

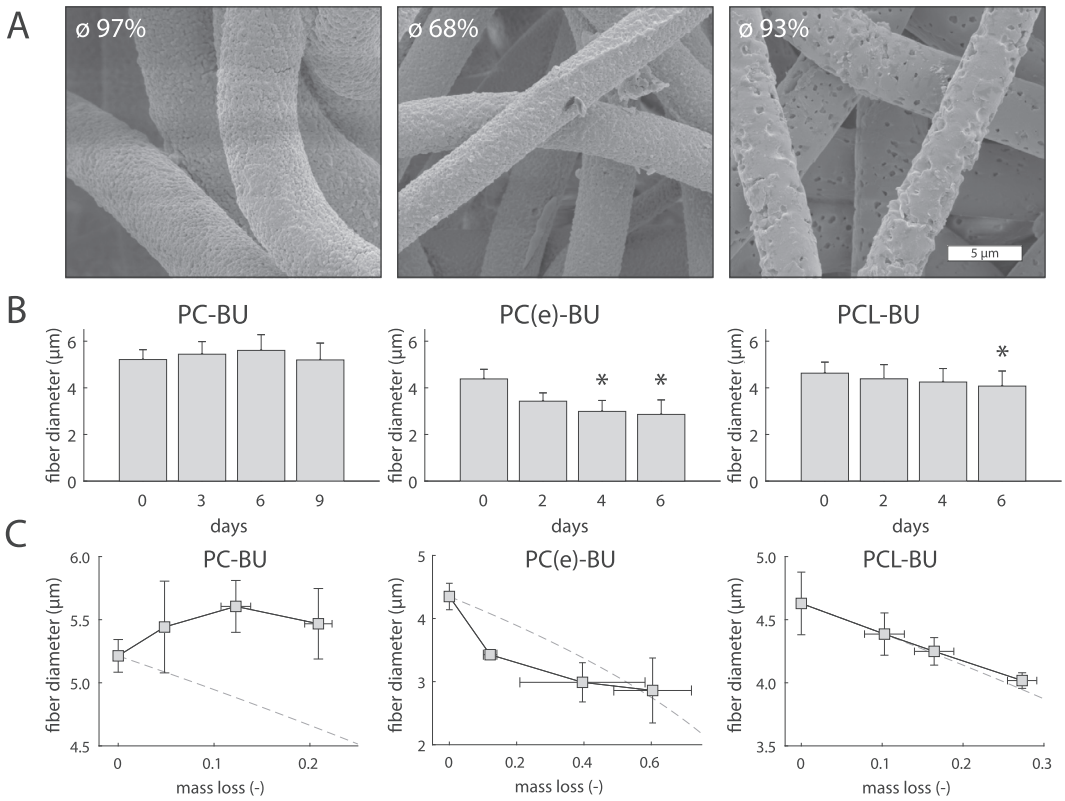

Fig. 5. Physical degradation on the fiber-scale. (A) Representative scanning electron microscopy images of electrospun BU-scaffolds after degradation (scale bar = 5 µm, percentage change in fiber diameter compared to day 0 is indicated in top left corner). (B) Quantification of fiber diameters of the BU-scaffolds during lipase incubation. (C) Relationship between fiber diameter and mass loss (the *dotted line* represents the expected relation if degradation occurs homogeneously due to surface erosion). *Asterisks* indicate statistical difference compared to day 0 ($^{*}p < 0.05$, see also Table SI3 in the Supplementary Information for the overall effect of incubation time).

PC-BU, PC(e)-BU, and PCL-BU are soluble in a range of solvents and can therefore be developed for solvent processing by electrospinning, resulting in fibrous scaffolds with non-linear and anisotropic mechanical properties. Scaffolds can be produced with about 5 µm fibers and open porous structures that allow infiltration of cells. One-pot produced BU-polyurethanes are less soluble, but can nevertheless be electrospun from HFIP to acquire scaffold meshes with (sub)micrometer fibers and relatively dense structures [31,32]. The PCL, PCL/PC and PC-BU-polyurethanes have also been examined in *in vitro* degradation assessments (on solid films exposed to PBS), and in *in vivo* degradation studies (on salt-leached scaffolds subcutaneously implanted in rats), and the results show a gradient in degradative behavior for the explored materials [29]. Although these investigations are related to this work, the experiments were not performed on electrospun scaffolds, precluding further direct comparisons.

In line with previous reported results on PCL-BU [26], PCL-BU scaffolds became more stiff with degradation (Fig. 7B, Table 3). We reasoned that the changes in mechanical properties were the result of changes at the network level (i.e., physical properties of fibers and scaffold) and at the material level (i.e., thermal properties and molecular weight). Indeed, the fibers in the PCL-BU scaffolds displayed surface erosion, as was monitored up to a substantial mass loss for the scaffold (Fig. 5C). At the material level, the hard block melting enthalpy and melting temperature (Fig. 6B, C) as well as the molecular weight (Fig. 6D) of PCL-BU tended to decrease with mass loss of the scaffold, indicating a deterioration in crystallinity [33] and, importantly, bulk degradation. This assessment is corroborated by SEM, showing affected rough-surfaced fibers with dents and pits (Fig. 5A), and with data from a comparable study that also showed a slight decrease in molecular weight of PCL-BU scaffolds after 30% mass loss as a result of lipase exposure [26]. Finally, the studied PCL-BU scaffolds showed a minor increase in the macroscopic density upon degradation (Fig. 4C), indicating a collapse of the fibrous network. Taken together, enzymatic hydrolytic degradation affected the polyester PCL-BU fibers from the outside and from the inside, and this presumably promoted the network to collapse, which in turn led to an overall stiffening of the scaffold.

It is important to notice that all scaffolds displayed anisotropic mechanical behavior at all time points. This anisotropic behavior is attributable to the higher degree of fiber alignment in the axial direction, especially for the PC(e)-BU and PCL-BU scaffolds, as a result of the electrospinning process (Table 2, Fig. SI2A). Interestingly, the stiffening effect in the PCL-BU scaffolds seemed to occur in the direction of the main fiber orientation (i.e., axial stiffening in axially aligned scaffolds and circumferential stiffening in circumferentially aligned scaffolds, Supplementary Information SI.7). The apparent relation between degradation and structural anisotropy adds an extra complexity to the design of scaffolds for *in situ* TE, which should be appropriately addressed with for example constitutive modeling [34]. This also holds for the non-linear mechanical behavior that these electrospun scaffolds exhibit. Due to the combined non-linearity and anisotropy, loading configurations are likely to vary during degradation, thereby influencing the regeneration process. The change in loading configuration during scaffold degradation could be captured with constitutive models as well, and used to optimize scaffold design.

The PC-BU scaffolds, on the other hand, maintained their mechanical properties during enzyme-accelerated hydrolytic

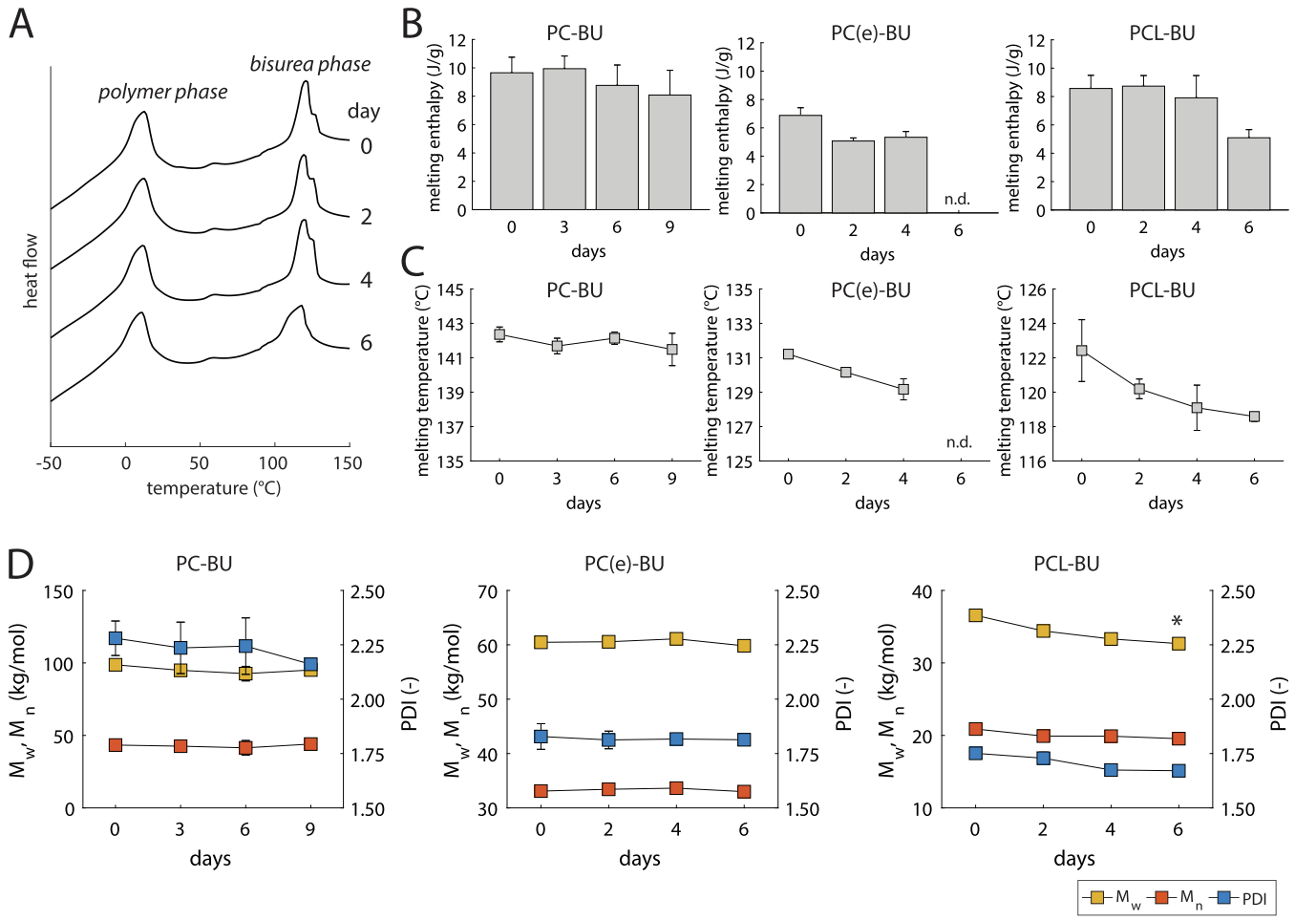

Fig. 6. Differential scanning calorimetry and gel permeation chromatography analysis. (A) Representative DSC curves (endothermic processes plotted as peaks) of electrospun PCL-BU scaffolds after lipase incubation. (B) Melting enthalpies and (C) melting temperatures of the bis-urea phase in BU-scaffolds after lipase incubation derived from the DSC curves (n.d., not determined). (D) Weight-averaged molecular weight M_w (*yellow*), number-averaged molecular weight M_n (*red*), and polydispersity index PDI (*blue*, *right* y-axis) of the BU-scaffolds during lipase incubation as determined with GPC. *Asterisks* indicate statistical difference compared to day 0 ($^*p < 0.05$, see also Table SI3 in the Supplementary Information for the overall effect of incubation time). (For interpretation of the references to colour in this figure legend, the reader is referred to the web version of this article.)

in vitro degradation (Fig. 7B, Table 3). This result is in line with previous work, albeit that degradation was only followed up to 5% mass loss [18]. At the network level, PC-BU fiber diameters increased (Fig. 5C) and scaffolds remained of constant thickness (Fig. 4B), despite the mass loss, suggesting that surface erosion in the PC-BU scaffolds is accompanied by swelling of the fibers with water. Swelling by absorption of water is known for PCL-based BU-polyurethanes, so it is not uncommon for BU-materials [35]. Chemical characterization of the PC-BU scaffolds indicated that the enzymes did not affect the material remaining in the fibers (Fig. 6), confirming that PC-BU solely degrades by surface erosion and not by bulk degradation. Consequently, the fibrous network gave stable mechanical moduli upon degradation up to about a 40% mass loss.

Finally, we introduced a new synthetic biomaterial, PC(e)-BU; a polymer that very closely resembles PC-BU with respect to its macromolecular structure. Surprisingly, however, PC(e)-BU scaffolds degrade at a rate that is more comparable to that of PCL-BU scaffolds, although PC(e)-BU initially deteriorates slower than PCL-BU (Fig. 3A). The ester bonds in PC(e)-BU are in close proximity to the stacking and crystallizing bis-urea (BU) groups, but apparently they are still quite accessible for cleavage by the lipase enzyme. At the material level, PC(e)-BU did not show signs for bulk degradation (Fig. 6D), which is similar to PC-BU. At the network level, the PC(e)-BU scaffolds were also more resembling the PC-BU scaffolds, as the fibers seemed to show surface erosion without signs of a collapsing network despite the significant reduction in fiber diameters (Figs. 4C and 5B, C). However, at extreme levels of degradation (ca. 80% mass loss), the PC(e)-BU scaffolds abruptly lose their mechanical properties, while remarkably the PCL-BU scaffolds retain their modulus (Table 3). In this respect, the performance of PC(e)-BU is inferior to that of PCL-BU, as for the latter the mechanical robustness is warranted over a broader degradation range.

Degradation of scaffolds *in vivo* is highly complex, involving the interplay between scaffold (e.g., fiber diameter, fiber alignment, pore size, and substrate stiffness), cells (e.g., macrophages and tissue producing cells [36–38]), and hemodynamics (e.g., shear stress and cyclic strain [28]). Our study highlights that through a simplification of these complex environments and a thorough examination of the physical, chemical, and mechanical changes during enzymatic degradation, it is possible to identify the degradation mechanisms of scaffolds that are designed for *in situ* TE applications. We therefore expect that this highly-controlled *in vitro* test-

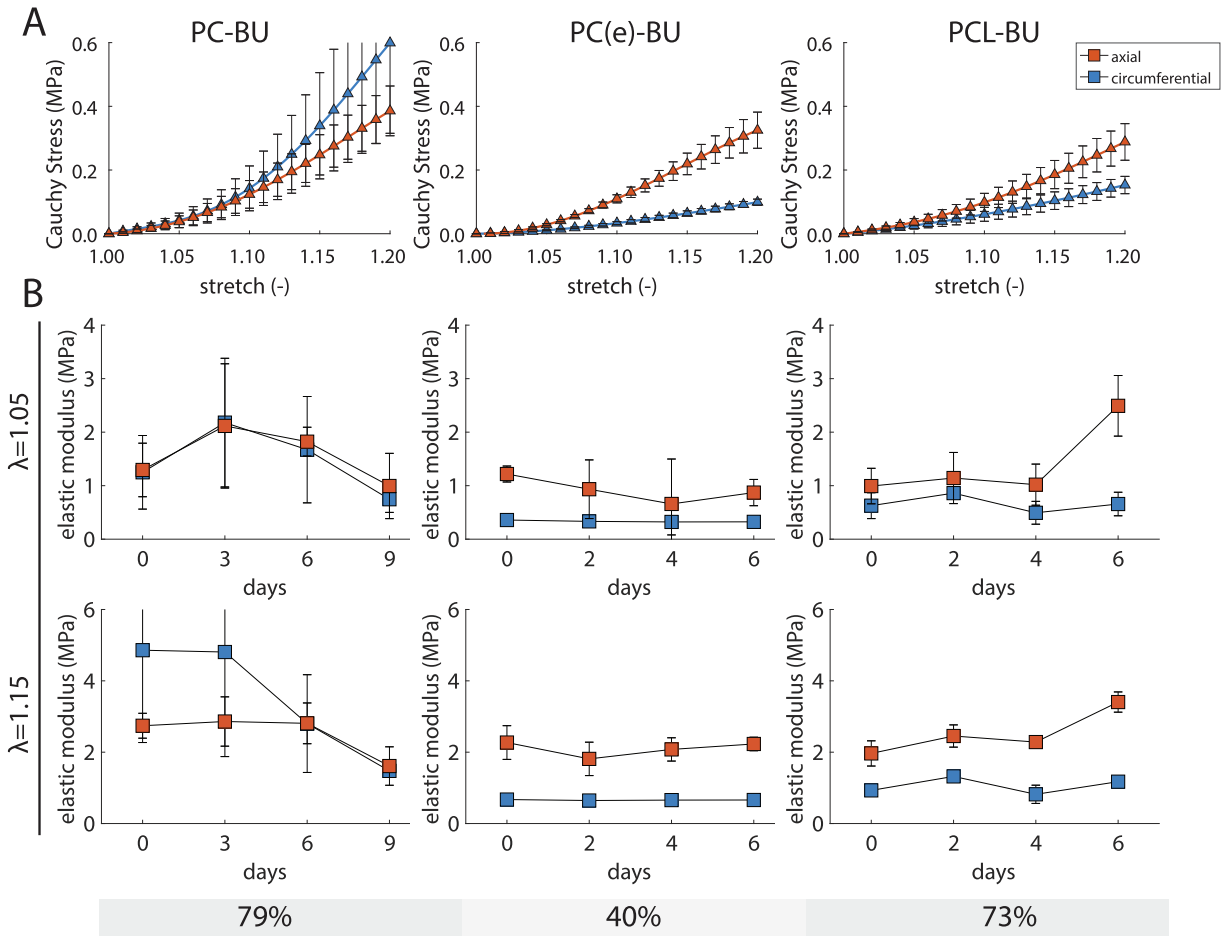

Fig. 7. Biaxial mechanical properties. (A) Averaged stress–stretch curves in axial (*red*) and circumferential (*blue*) direction of electrospun BU-scaffolds prior to degradation. (B) Quantification of elastic modulus (defined as the slope at 1.05 stretch (*top row*) and 1.15 stretch (*bottom row*) in the stress–stretch curve) of the scaffolds during lipase incubation. The *bottom line* shows the remaining mass of the tested scaffolds at the last time point of the mechanical analysis (see also Table SI3 in the Supplementary Information for the overall effect of incubation time). (For interpretation of the references to colour in this figure legend, the reader is referred to the web version of this article.)

Table 3
Biaxial mechanical properties of extremely degraded scaffolds.

Degradation read-out	Material group		
	PC-BU	PC(e)-BU	PCL-BU
Remaining mass (%)	59.8 ± 1.18	17.3 ± 2.1	23.7 ± 5.15
Elastic modulus (MPa, circumferential)			
λ = 1.05	0.68 ± 0.07	<0.17*	2.17 ± 0.63
λ = 1.15	1.48 ± 0.20	<0.13*	2.24 ± 0.39
Elastic modulus (MPa, axial)			
λ = 1.05	1.21 ± 0.48	<0.01*	5.37 ± 1.00
λ = 1.15	2.19 ± 0.03	<0.10*	4.40 ± 0.17

* Due to sample breakdown, only n = 1 sample was measurable.

ing approach can be useful to also reveal the degradation mechanisms of materials in general that relate to, for example, oxidation and physical loads [26].

5. Conclusions and outlook

We have shown that electrospun vascular scaffolds made from a set of sequence-controlled BU-modified biomaterials with varying amounts of ester groups in the polymer backbone are degraded through different mechanisms when exposed to lipase. PC-BU and PC(e)-BU polycarbonate scaffolds, with respectively a low and intermediate susceptibility to degradation, degrade through surface erosion, resulting in maintenance of the scaffold's mechanical properties. PCL-BU polyester scaffolds, with a high susceptibility to degradation, degrade through surface erosion and some bulk degradation, which ultimately is accompanied by a network collapse, resulting in overall stiffening of the scaffold. Overall, it is observed that enzymatic hydrolytic degradation of electrospun scaffolds can be slowed down effectively when PC-BU is used, a material with only bis-urea (BU) and carbonate groups and without ester or urethane moieties. These results aid in the selection of electrospun biodegradable polymeric scaffolds for *in situ* TE, for instance for the preparation of small-diameter vascular substitutes [6,7,39].

The introduction of PC(e)-BU to the set of BU-modified supramolecular polymers opens new opportunities to further tune the degradation kinetics of scaffold implants. In contrast to polymers in general, PC(e)-BU and PC-BU can, due to their macromolecular similarity, be combined to acquire an intimately mixed polymer blend (Supplementary Information SI.3). Since their degradation mechanisms are alike, but their degradation rates vary, mixtures of these polymers are expected to resorb at inter-

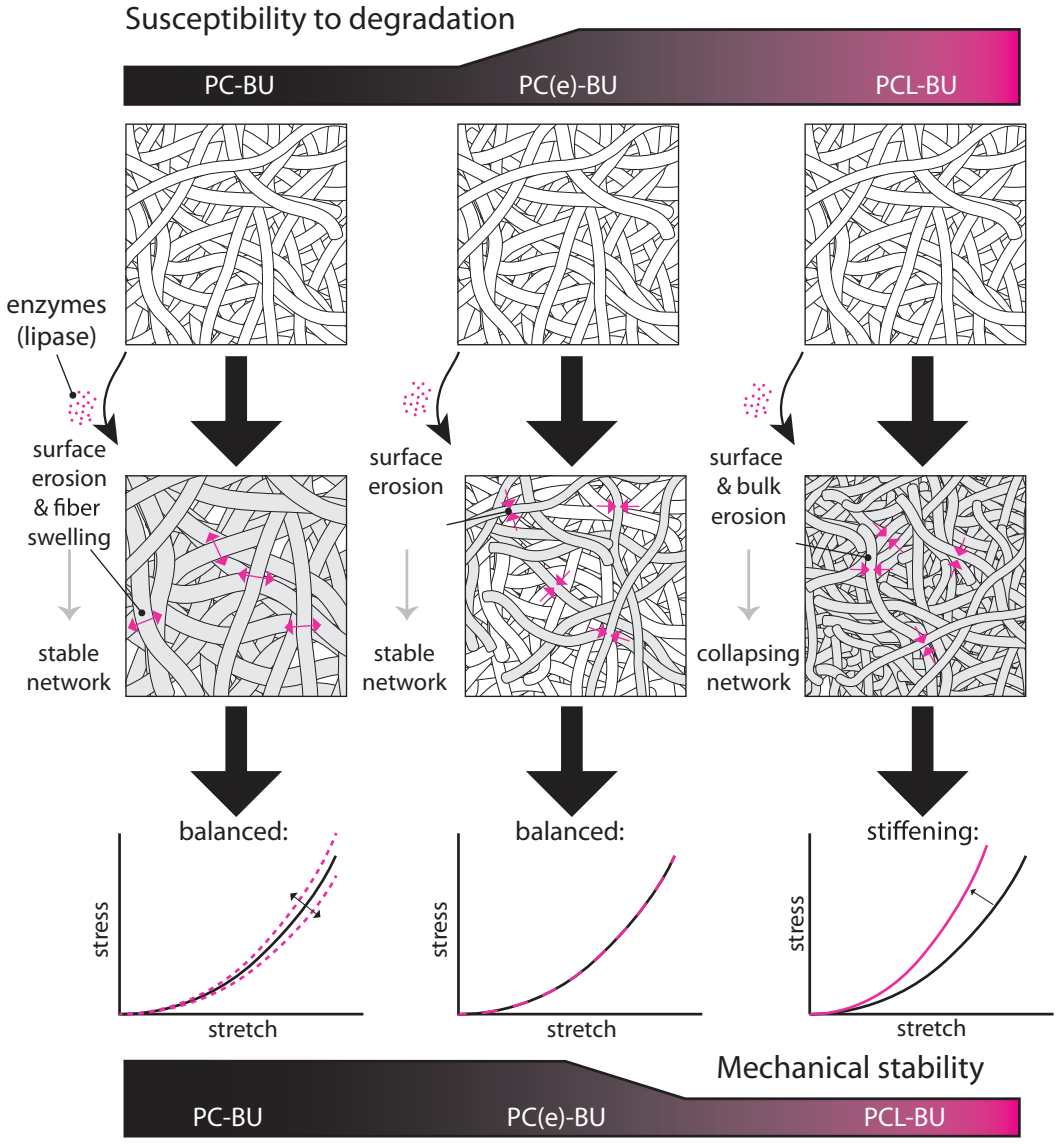

Fig. 8. Schematic illustrating the proposed degradation mechanisms for scaffolds of the three tested sequence-controlled BU-materials with varying susceptibilities to enzymatic degradation.

mediate rates. This mix-and-match approach illustrates that the class of supramolecular polymers continues to represent a promising group of materials for use in (vascular) TE approaches in particular, and biomedical applications in general.

Acknowledgments

The authors would like to thank Andrea di Luca and Wojciech Szymczyk for their help with electrospinning of the scaffolds and Hannah Brouwer for her assistance with mass loss and thickness measurements. This study is financially supported by ZonMw as part of the LSH 2Treat program (436001003) and the Dutch Kidney Foundation (14a2d507). We also gratefully acknowledge funding for the Gravitation Program "Materials Driven Regeneration" by the Netherlands Organization for Scientific Research (024.003).

Author contributions

E.E.v.H., R.D., N.A.K, P.Y.W.D., and C.V.C.B. conceptualized the study. S.H.M.S, M.H.C.J., and H.M.J. designed, developed and synthesized the polymers. E.E.v.H. and R.D. performed the experiments and analyzed the data. B.D.I. performed the chemical analyses. E.E.v.H. and R.D. wrote the article. All authors were involved in the review and editing of the article. N.A.K, A.I.P.M., P.Y.W.D., and C.V.C.B. supervised the project. P.Y.W.D. and C.V.C.B. managed the research and acquired funding to execute the project.

Appendix A. Supplementary data

Supplementary data to this article can be found online at https://doi.org/10.1016/j.actbio.2019.05.037.

References

[1] E.J. Benjamin, S. Virani, C. Callaway, A. Chamberlain, A. Chang, S. Cheng, S. Chiuve, M. Cushman, F. Delling, R. Deo, S. de Ferranti, Heart disease and stroke statistics—2018 update: a report from the American Heart Association, Circulation 137 (2018) e67–e492.

[2] J.H. Lawson, M.H. Glickman, M. Ilzecki, T. Jakimowicz, A. Jaroszynski, E.K. Peden, A.J. Pilgrim, H.L. Prichard, M. Guziewicz, S. Przywara, J. Szmidt, J. Turek, W. Witkiewicz, N. Zapotoczny, T. Zubilewicz, L.E. Niklason, Bioengineered

human acellular vessels for dialysis access in patients with end-stage renal disease: two phase 2 single-arm trials, Lancet 387 (2016) 2026–2034, https://doi.org/10.1016/S0140-6736(16)00557-2.
[3] J. Chlupác, E. Filová, L. Bačáková, Blood vessel replacement: 50 years of development and tissue engineering paradigms in vascular surgery, Physiol. Res. 58 (2009) 119–140.
[4] P. Collins, C.M. Webb, C.F. Chong, N.E. Moat, Radial artery versus saphenous vein patency randomized trial: five-year angiographic follow-up, Circulation 117 (2008) 2859–2864, https://doi.org/10.1161/CIRCULATIONAHA.107.736215.
[5] H. Haruguchi, S. Teraoka, Intimal hyperplasia and hemodynamic factors in arterial bypass and arteriovenous grafts: a review, J. Artif. Org. 6 (2003) 227–235, https://doi.org/10.1007/s10047-003-0232-x.
[6] S. Li, D. Sengupta, S. Chien, Vascular tissue engineering: from in vitro to in situ, Wiley Interdiscip. Rev. Syst. Biol. Med. 6 (2014) 61–76, https://doi.org/10.1002/wsbm.1246.
[7] T.B. Wissing, V. Bonito, C.V.C. Bouten, A.I.P.M. Smits, Biomaterial-driven in situ cardiovascular tissue engineering—a multi-disciplinary perspective, NPJ Regen. Med. 2 (2017) 1–19, https://doi.org/10.1038/s41536-017-0023-2.
[8] S. Tara, H. Kurobe, M.W. Maxfield, K.A. Rocco, T. Yi, Y. Naito, C.K. Breuer, T. Shinoka, Evaluation of remodeling process in small-diameter cell-free tissue-engineered arterial graft, J. Vasc. Surg. (2014) 1–10, https://doi.org/10.1016/j.jvs.2014.03.011.
[9] S. Lyu, D. Untereker, Degradability of polymers for implantable biomedical devices, Int. J. Mol. Sci. 10 (2009) 4033–4065, https://doi.org/10.3390/ijms10094033.
[10] L. Pastorino, F. Pioli, M. Zilli, A. Converti, C. Nicolini, Lipase-catalyzed degradation of poly(ε-caprolactone), Enzyme Microb. Technol. 35 (2004) 321–326, https://doi.org/10.1016/j.enzmictec.2004.05.005.
[11] H. Peng, J. Ling, J. Liu, N. Zhu, X. Ni, Z. Shen, Controlled enzymatic degradation of poly(ε-caprolactone)-based copolymers in the presence of porcine pancreatic lipase, Polym. Degrad. Stab. 95 (2010) 643–650, https://doi.org/10.1016/j.polymdegradstab.2009.12.005.
[12] P.Y.W. Dankers, M.C. Harmsen, L.A. Brouwer, M.J.A. van Luyn, E.W. Meijer, A modular and supramolecular approach to bioactive scaffolds for tissue engineering, Nat. Mater. 4 (2005) 568–574, https://doi.org/10.1038/nmat1418.
[13] G.C. Van Almen, H. Talacua, B.D. Ippel, B.B. Mollet, M. Ramaekers, M. Simonet, A.I.P.M. Smits, C.V.C. Bouten, J. Kluin, P.Y.W. Dankers, Development of non-cell adhesive vascular grafts using supramolecular building blocks, Macromol. Biosci. 16 (2016) 350–362.
[14] V. Bonito, A.I.P.M. Smits, O.J.G.M. Goor, B.D. Ippel, A. Driessen-Mol, T.J.A.G. Münker, A.W. Bosman, T. Mes, P.Y.W. Dankers, C.V.C. Bouten, Modulation of macrophage phenotype and protein secretion via heparin-IL-4 functionalized supramolecular elastomers, Acta Biomater. 71 (2018) 247–260, https://doi.org/10.1016/j.actbio.2018.02.032.
[15] B.D. Ippel, H.M. Keizer, P.Y.W. Dankers, Supramolecular antifouling additives for robust and efficient functionalization of elastomeric materials: molecular design matters, Adv. Funct. Mater. 1805375 (2018) 1–11, https://doi.org/10.1002/adfm.201805375.
[16] L. Brunsveld, J. Folmer, E. Meijer, R. Sijbesma, Supramolecular polymers, Chem. Rev. 101 (2001) 4071–4097, https://doi.org/10.1002/9783527674107.ch30.
[17] M.J. Webber, E.A. Appel, E.W. Meijer, R. Langer, Supramolecular biomaterials, Nat. Mater. 15 (2015) 13–26, https://doi.org/10.1038/nmat4474.
[18] J. Kluin, H. Talacua, A.I.P.M. Smits, M.Y. Emmert, M.C.P. Brugmans, E.S. Fioretta, P.E. Dijkman, S.H.M. Söntjens, R. Duijvelshoff, S. Dekker, M.W.J.T. Janssen-van den Broek, V. Lintas, A. Vink, S.P. Hoerstrup, H.M. Janssen, P.Y.W. Dankers, F.P.T. Baaijens, C.V.C. Bouten, In situ heart valve tissue engineering using a bioresorbable elastomeric implant – from material design to 12 months follow-up in sheep, Biomaterials 125 (2017) 101–117, https://doi.org/10.1016/j.biomaterials.2017.02.007.
[19] R. Duijvelshoff, N. van Engeland, K. Gabriels, S. Söntjens, A. Smits, P. Dankers, C. Bouten, Host response and neo-tissue development during resorption of a fast degrading supramolecular electrospun arterial scaffold, Bioengineering 5 (2018) 61, https://doi.org/10.3390/bioengineering5030061.
[20] E. Wisse, A.J.H. Spiering, E.N.M. van Leeuwen, R.A.E. Renken, P.Y.W. Dankers, L. A. Brouwer, M.J.A. van Luyn, M.C. Harmsen, N.A.J.M. Sommerdijk, E.W. Meijer, Molecular recognition in poly(ε-caprolactone)-based thermoplastic elastomers, Biomacromolecules 7 (2006) 3385–3395, https://doi.org/10.1021/bm060688t.
[21] J.-C. Tille, S. de Valence, D. Mandracchia, B. Nottelet, F. Innocente, R. Gurny, M. Möller, B. Walpoth, Histologic assessment of drug-eluting grafts related to implantation site, J. Dev. Biol. 4 (2016) 11, https://doi.org/10.3390/jdb4010011.
[22] Y. Dong, S. Liao, M. Ngiam, C.K. Chan, S. Ramakrishna, Degradation behaviors of electrospun resorbable polyester nanofibers, Tissue Eng. Part B: Rev. 15 (2009) 333–351, https://doi.org/10.1089/ten.teb.2008.0619.
[23] E. Wisse, A.J.H. Spiering, F. Pfeifer, G. Portale, H.W. Siesler, E.W. Meijer, Segmental orientation in well-defined thermoplastic elastomers containing supramolecular fillers, Macromolecules 42 (2009) 524–530, https://doi.org/10.1021/ma801668k.
[24] L. Soletti, Y. Hong, J. Guan, J.J. Stankus, M.S. El-Kurdi, W.R. Wagner, D.A. Vorp, A bilayered elastomeric scaffold for tissue engineering of small diameter vascular grafts, Acta Biomater. 6 (2010) 110–122, https://doi.org/10.1016/j.actbio.2009.06.026.
[25] E.M. Christenson, S. Patel, J.M. Anderson, A. Hiltner, Enzymatic degradation of poly(ether urethane) and poly(carbonate urethane) by cholesterol esterase, Biomaterials 27 (2006) 3920–3926, https://doi.org/10.1016/j.biomaterials.2006.03.012.
[26] M.C.P. Brugmans, S.H.M. Sntjens, M.A.J. Cox, A. Nandakumar, A.W. Bosman, T. Mes, H.M. Janssen, C.V.C. Bouten, F.P.T. Baaijens, A. Driessen-Mol, Hydrolytic and oxidative degradation of electrospun supramolecular biomaterials: in vitro degradation pathways, Acta Biomater. 27 (2015) 21–31, https://doi.org/10.1016/j.actbio.2015.08.034.
[27] E.E. van Haaften, T.B. Wissing, M.C.M. Rutten, J.A. Bulsink, K. Gashi, M.A.J. van Kelle, A.I.P.M. Smits, C.V.C. Bouten, N.A. Kurniawan, Decoupling the effect of shear stress and stretch on tissue growth & remodeling in a vascular graft ten. TEC.2018.0104, Tissue Eng. Part C: Methods 24 (2018), https://doi.org/10.1089/ten.TEC.2018.0104.
[28] E.E. van Haaften, C.V.C. Bouten, N.A. Kurniawan, Vascular mechanobiology: towards control of in situ regeneration, Cells 6 (2017) 1–24, https://doi.org/10.3390/cells6030019.
[29] Y. Hong, J. Guan, K.L. Fujimoto, R. Hashizume, A.L. Pelinescu, W.R. Wagner, Tailoring the degradation kinetics of poly (ester carbonate urethane) urea thermoplastic elastomers for tissue engineering scaffolds, Biomaterials 31 (2010) 4249–4258, https://doi.org/10.1016/j.biomaterials.2010.02.005.
[30] A. D'Amore, S.K. Luketich, G.M. Raffa, S. Olia, G. Menallo, A. Mazzola, F. D'Accardi, T. Grunberg, X. Gu, M. Pilato, M.V. Kameneva, V. Badhwar, W.R. Wagner, Heart valve scaffold fabrication: bioinspired control of macro-scale morphology, mechanics and micro-structure, Biomaterials 150 (2018) 25–37, https://doi.org/10.1016/j.biomaterials.2017.10.011.
[31] R. Hashizume, K.L. Fujimoto, Y. Hong, N.J. Amoroso, K. Tobita, T. Miki, B.B. Keller, M.S. Sacks, W.R. Wagner, Morphological and mechanical characteristics of the reconstructed rat abdominal wall following use of a wet electrospun biodegradable polyurethane elastomer scaffold, Biomaterials 31 (2010) 3253–3265, https://doi.org/10.1016/j.biomaterials.2010.01.051.
[32] J.J. Stankus, J. Guan, W.R. Wagner, Fabrication of biodegradable elastomeric scaffolds with sub-micron morphologies, J. Biomed. Mater. Res. Part A 70 (2004) 603–614, https://doi.org/10.1002/jbm.a.30122.
[33] A.W.T. Shum, A.F.T. Mak, Morphological and biomechanical characterization of poly(glycolic acid) scaffolds after in vitro degradation, Polym. Degrad. Stab. 81 (2003) 141–149, https://doi.org/10.1016/S0141-3910(03)00083-1.
[34] G. Limbert, R. Omar, H. Krynauw, D. Bezuidenhout, T. Franz, The anisotropic mechanical behaviour of electro-spun biodegradable polymer scaffolds: experimental characterisation and constitutive formulation, J. Mech. Behav. Biomed. Mater. 53 (2016) 21–39, https://doi.org/10.1016/j.jmbbm.2015.07.014.
[35] J. Guan, M.S. Sacks, E.J. Beckman, W.R. Wagner, Synthesis, characterization, and cytocompatibility of elastomeric, biodegradable poly(ester-urethane) ureas based on poly(caprolactone) and putrescine, J. Biomed. Mater. Res. 61 (2001) 493–503.
[36] A. Mantovani, S.K. Biswas, M.R. Galdiero, A. Sica, M. Locati, Macrophage plasticity and polarization in tissue repair and remodelling, J. Pathol. 229 (2013) 176–185, https://doi.org/10.1002/path.4133.
[37] K. Garg, N.A. Pullen, C. Oskeritzian, J. Ryan, G. Bowlin, Macrophage functional polarization (M1/M2) in response to varying fiber and pore dimensions of electrospun scaffolds, Biomaterials 34 (2013) 4439–4451, https://doi.org/10.1016/j.biomaterials.2013.02.065.MACROPHAGE.
[38] V. Ballotta, A. Driessen-Mol, C.V.C. Bouten, F.P.T. Baaijens, Strain-dependent modulation of macrophage polarization within scaffolds, Biomaterials 35 (2014) 4919–4928, https://doi.org/10.1016/j.biomaterials.2014.03.002.
[39] K.A. Rocco, M.W. Maxfield, C.A. Best, E.W. Dean, C.K. Breuer, *In vivo* applications of electrospun tissue-engineered vascular grafts: a review, Tissue Eng. Part B: Rev. 20 (2014) 628–640, https://doi.org/10.1089/ten.teb.2014.0123.